JOURNAL OF GEOPHYSICAL RESEARCH, VOL. 111, D14303, doi:10.1029/2005JD006719, 2006

Aircraft validation of clear air absorption models at millimeter wavelengths (89–183 GHz)

Tim J. Hewison[1]

Received 28 September 2005; revised 28 March 2006; accepted 19 April 2006; published 20 July 2006.

[1] Measurements with an airborne microwave radiometer are used to validate absorption models in clear air at frequencies used in satellite microwave humidity sounders, such as AMSU-B and MHS. The data set includes 33 profiles of radiometric and in situ observations ranging from the tropics to the high arctic. In cold, dry conditions the MPM and Rosenkranz models were found to underestimate the observed downwelling radiances near the surface in window channels dominated by the water vapor continuum. The models' absorption coefficient is calculated and found to be strongly deficient compared to observations in layers of low specific humidity. For medium humidity, the models' negative bias persists at 89 GHz and becomes statistically significant, but reduces at higher frequencies. Previously, the radiometer calibration had been adjusted to fit modeled radiances during high-level flight; this approach has been revised in the light of these findings and a tip curve method applied. Possible spectroscopic reasons for the models' deficits are suggested, including the underestimation of continuum terms or the extrapolation of oxygen line coupling coefficients to low temperatures. The impacts for operational use of radiative transfer models are discussed.

Citation: Hewison, T. J. (2006), Aircraft validation of clear air absorption models at millimeter wavelengths (89–183 GHz), *J. Geophys. Res.*, *111*, D14303, doi:10.1029/2005JD006719.

1. Introduction

[2] Water vapor plays a critical role in meteorology and climatology, yet is one of the most difficult atmospheric parameters to measure accurately. During 1999, the UK Met Office conducted a campaign named MOTH (Measurement Of Tropospheric Humidity) to improve our understanding of water vapor observations. Data from an airborne interferometer during MOTH have been used to validate models in the infrared [*Taylor et al.*, 2003]. This paper reports how data from this campaign and others have been used to validate microwave absorption models at 89–183 GHz, where absorption is dominated by water vapor. These models are needed for the assimilation of data from satellite microwave humidity sounders into Numerical Weather Prediction (NWP). These instruments are now used to provide global information on vertical humidity profiles, yet there is little data available to validate their performance in real tropospheric conditions.

[3] The high spatial and temporal variability of water vapor complicates the accurate comparisons of satellite radiances with in situ data. Several authors have presented validation of absorption models by comparing radiances observed by ground-based microwave radiometers and forward modeled coincident radiosonde profiles. The models referred to are outlined in section 2.

[4] *Cimini et al.* [2003] compared observations of ground-based microwave radiometers at 20–30 GHz with coincident radiosonde profiles in clear air using the Ros98 [*Rosenkranz*, 1998] absorption model. They found a dry bias of ~5% using Vaisala RS80 humidity sensors. This was much reduced with RS90 sensors. *Westwater et al.* [2003] used similar radiometers in the tropics, but found variability in radiosonde humidity measurements dominated differences between absorption models at 23.8 GHz. They showed that MPM87 [*Liebe and Layton*, 1987] fitted observations better than Ros98 at 31.4 GHz, which is dominated by the water vapor continuum. Earlier work [*Westwater et al.*, 2001] had shown that Ros98 best fitted observations at 31.4 GHz in cold, dry arctic conditions.

[5] *English et al.* [1994, 1995] used an earlier version of the Microwave Airborne Radiometer Scanning System (MARSS) used in this study to validate water vapor continuum models in window channels at 89 and 157 GHz. They found all models underestimated the downwelling brightness temperatures in the tropics (except MPM93), but overestimated in subarctic conditions. They proposed a modification to the temperature dependence of the MPM89 water vapor continuum to match their observations.

[6] Many of the models' line parameters are based on laboratory measurements for temperatures above 0°C. To apply these to atmospheric conditions, they are extrapolated to lower temperatures, which amplifies their errors. *Boukabara et al.* [2005] showed that a 10% change in oxygen line coupling coefficients can produce changes of ~1.5 K and ~0.5 K in the brightness temperatures seen by a nadir viewing satellite at 89 and 150 GHz, respectively. This perturbation is within the expected uncertainty of the original measurements by *Liebe et al.* [1992]. However, *Rosenkranz* [2005] has since pointed out that care is needed

[1]Met Office, University of Reading, Reading, UK.

Table 1. Water Vapor Continuum Parameters Used in Equation (1) by Seven Models

Model	C_s, $\frac{dB/km}{hPa^2GHz^2}$	n_s	C_f, $\frac{dB/km}{hPa^2GHz^2}$	n_f
MPM87	6.50×10^{-8}	7.8	2.06×10^{-9}	0.0
MPM89	6.50×10^{-8}	7.5	2.06×10^{-9}	0.0
MPM93[a]	7.73×10^{-8}	4.55	2.53×10^{-9}	1.55
Ros98	7.82×10^{-8}	4.5	2.36×10^{-9}	0.0
Ros03	7.82×10^{-8}	4.5	2.36×10^{-9}	0.0
M&T03[b]	7.82×10^{-8}	4.5	1.59×10^{-9}	1.98
CKD2.4.1	4.63×10^{-8}	3.78	2.99×10^{-9}	0.0

[a]Approximation of pseudo-line for $\nu < 800$ GHz.
[b]The foreign-broadening has a $\nu^{2.059}$ dependence in M&T03.

to ensure modifications are physically consistent, as the uncertainties are highly correlated.

[7] This paper first follows the method of comparing observed and modeled downwelling radiances near the surface. However, these radiances are dominated by emission from water vapor at relatively high temperatures and pressures. Radiances measured by satellite radiometers are also sensitive to emission from water vapor at lower pressures and temperatures. Absorption in these conditions may be validated using coincident measurements from airborne microwave radiometers and in situ sensors to provide profile information. This study reveals large differences in absorption coefficients calculated in these conditions.

2. Absorption Models

[8] In the troposphere, clear air absorption at microwave and millimeter wavelengths is dominated by oxygen and water vapor. Oxygen produces strong resonant absorption due to transitions in the magnetic dipole spin-rotation band around 60 GHz. Rotational transitions of the electric dipole of water vapor produce resonant absorption lines extending from the microwave to submillimeter wavelengths, including 22.235 GHz and 183.31 GHz.

[9] The remainder of this part of the spectrum is dominated by a continuum component of the water vapor absorption. Although many theories have been developed to explain the process responsible for the water vapor continuum, it is usually represented as an empirical term used to fit observations to the theoretically based resonant terms. It is generally divided into two contributions, which are self- and foreign-broadened, because of collisions of water vapor molecules with molecules of the same species or other gases, respectively. Absorption by the water vapor continuum, α_c, at frequency, ν, is generally represented as [*Rosenkranz*, 1998]:

$$\alpha_C = \nu^2\Theta^3\left(C_s \cdot P_{H_2O}^2 \cdot \Theta^{n_s} + C_f \cdot P_d \cdot P_{H_2O} \cdot \Theta^{n_f}\right) \quad (1)$$

where $\Theta = (300\ \mathrm{K})/T$ is a dimensionless variable related to the temperature, T, P_{H2O} is the vapor pressure, P_d is the dry air pressure, and the parameters C_s, n_s, C_f and n_f describe the coefficients and exponents of the temperature dependence of the self- and foreign-broadened parts of the water vapor continuum, respectively, given in Table 1.

[10] There are numerous ozone lines at millimeter wavelengths, including four in the passbands of the 183 GHz channels. Their influence was investigated using a line-by-line transmission model [*Edwards*, 1992]. Emission from stratospheric ozone in a standard atmosphere was found to contribute less than 0.6 K to the brightness temperature of these channels. It was neglected from further analysis.

[11] The oxygen spin-rotation band also includes nonresonant transitions leading to absorption that is relatively weak at 60 GHz, but that also contributes to line coupling in the resonant region. As for nitrogen, otherwise inactive, there is pressure induced absorption, which becomes significant above 100 GHz in very dry conditions. Although the strength of these terms vary between the models, their impact is small.

[12] The differences between the models pertinent to this study are discussed in the following subsections. A more general discussion is given by *Rayer* [2001]. Figure 1 gives an example of absorption coefficients calculated for typical midtropospheric conditions. The curves in this plot represent the absorption spectrum predicted by six models and shaded areas denote the passbands of MARSS' channels. The differences between the models shown are not general, and depend on temperature, pressure, humidity and frequency.

2.1. MPM87 [*Liebe and Layton*, 1987]

[13] The clear air absorption part of the Millimeter-wave Propagation Model, MPM87 includes 30 water vapor lines and 44 oxygen lines all in the range 20 GHz to 1 THz, based on theoretical values and a Van-Vleck Weisskopf shape function. These are supplemented by an empirically derived water vapor continuum, fitted to laboratory observations at 138 GHz. However, these observations were limited to 282–316 K, and must be extrapolated for typical atmospheric conditions. Additional terms represent the nonresonant absorption due to the Debye spectrum of oxygen below 10 GHz and the pressure-induced nitrogen absorption above 100 GHz, which can become a significant contribution to the overall absorption in low humidity.

2.2. MPM89 [*Liebe*, 1989]

[14] The 1989 revision of MPM modified the parameters describing the 183 GHz water vapor line, fitting the

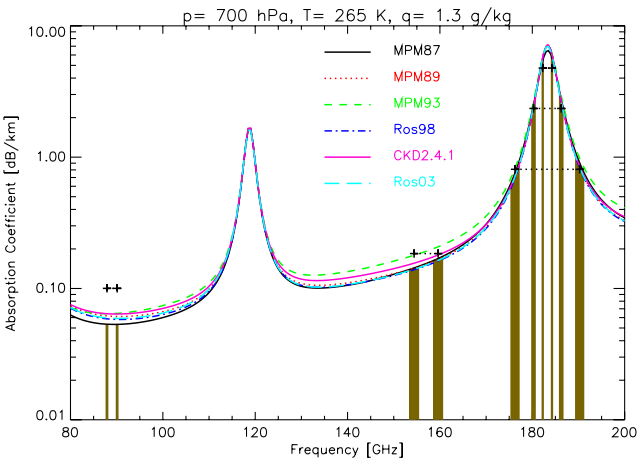

Figure 1. Atmospheric absorption spectrum for typical midtroposphere conditions from seven models. Shaded areas represent passbands of MARSS' channels, shown in Table 2. Points linked with horizontal lines indicate average absorption measured in these conditions.

pressure broadened line width with four parameters, instead of one. Other components are the same as MPM87 for the purposes of this study.

2.3. MPM93 [*Liebe et al.*, 1993]

[15] This version of MPM, has 34 water vapor lines between 20–1000 GHz, defined in a slightly different manner from MPM89. The 183 GHz line is 8.5% wider and 5% stronger than in MPM89. The water vapor continuum absorption is formulated as a ''pseudo-line'' near 2 THz, and has a different temperature dependence, based on newer observations. Like its predecessors, MPM93 includes 44 oxygen lines. Updated oxygen line coupling appeared in MPM92 oxygen model [*Liebe et al.*, 1992] and were then used in MPM93 with widths and line coupling increased by 5% and 15% respectively. The nitrogen continuum is also few% stronger than in MPM89 at the frequencies of this study.

2.4. Ros98 [*Rosenkranz*, 1998]

[16] Ros98 uses 15 water vapor line parameters, which are very similar to the strongest lines used in MPM89. The other half of the lines have been omitted as they were judged to have negligible impact. Rosenkranz's investigations suggested a range of observations could be best modeled by using a water vapor continuum with a combination of MPM87's foreign-broadened component, and MPM93's self-broadened component. However, the water vapor lines used were truncated at ±750 GHz, so C_f and C_s were increased 15% and 3%, respectively to compensate. This model uses the same oxygen line parameters as MPM93, except at submillimeter frequencies, where values from the HITRAN [*Rothman et al.*, 1992] database were used. The nonresonant nitrogen absorption used with this model [*Rosenkranz*, 1993] is ~10% higher than in MPM89.

2.5. Ros03 (P. W. Rosenkranz, Personal Communication, 2003)

[17] In 2003, Rosenkranz updated his water vapor model to include recent measurements and pressure line shift mechanism described by *Tretyakov et al.* [2004]. He also corrected some line intensities and revised the width of the 425 GHz oxygen line [*Krupnov et al.*, 2002] and the line coupling and width of the 1- line at 118.75 GHz [*Tretyakov et al.*, 2004]. He has also adopted recent submillimeter observations [*Pardo et al.*, 2001] suggesting the strength of the dry nitrogen absorption should be increased by 29%. The intensity and air-broadened width of the 183 GHz line are 0.264% and 2% higher in Ros03 than Ros98. Other parameters of this line are unchanged.

2.6. M&T03 [*Ma and Tipping*, 2003]

[18] *Ma and Tipping* [2003] presented a theoretical model to describe the foreign-broadened water vapor continuum at millimeter wavelengths. They fitted this to an empirical function of the form of equation (1). Like MPM93, it has a much stronger temperature dependence than other models, but it also has a $\nu^{2.059}$ frequency dependence. In this study, this has been substituted for the foreign-broadened water vapor continuum in Ros98 and is referred to as M&T03. In all other respects, this is the same model as Ros98, but with a 1000 GHz cutoff imposed in the calculation of spectral line contributions (although this makes negligible difference for the channels used in this study).

2.7. CKD2.4.1 [*Clough et al.*, 1989]

[19] Rosenkranz's adoption of the 750 GHz cutoff in calculation of spectral line absorption is consistent with that of HITRAN. This allows the CKD water vapor continuum to be directly substituted into Ros98 to compare the effectiveness of both models. In all other respects the model referred to in this study as CKD2.4.1 is the same as Ros98. The coefficients of v2.4.1 of the CKD continuum are given in Table 1.

3. Measurements

[20] The results presented in this paper are derived from data collected by instruments described below mounted on the Met Office C-130 research aircraft.

3.1. Flights Used in This Study

[21] During 1999, the UK Met Office conducted two field experiments, with the objective of the Measurement of Tropospheric Humidity (MOTH) [*Taylor et al.*, 2003]. The first of these was based on Ascension Island in the South Atlantic during April-May, where Integrated Water Vapor (IWV) column amounts from 29–42 kg/m^2 were measured by aircraft instruments during profiles. The second took place over the Baltic Sea during December, where IWV was much lower (as low as 4.1 kg/m^2).

[22] These flights comprised a stack of straight and level runs flown at various altitudes, in an area identified as likely to remain free of cloud for the duration of a sortie (typically 6 hours). Long, staggered ascents and descents, known as profiles, were also flown to acquire profiles of temperature and humidity for input to the radiative transfer models. These typically took only 40 min from minimum altitude (15 m) to the aircraft ceiling (7.5 km in the tropics, 9.5 km in the arctic) and were usually staggered to extend ~60 km in the horizontal.

[23] Profiles were also taken from other flights in clear sky conditions, including flights in Germany in May 1999, near Windhoek and Cape Verde in September 2000, and near Svalbard in March 2001. An additional flight was conducted near the UK in December 2000. In this case, a slow spiral ascent was flown from 15 m to 9.5 km at a constant 12° bank, over 2 hours.

3.2. MARSS Instrument

[24] The primary instrument used in this study is the Microwave Airborne Radiometer Scanning System (MARSS), which has channels designed to match some of those on the Advanced Microwave Sounding Unit (AMSU), which operate on the NOAA polar orbiting satellites. MARSS' characteristics for this data set are summarized in Table 2.

[25] MARSS' pod (shown in Figure 2) is mounted external to the aircraft's fuselage. This contains a scan mirror, which reflects scenes of nine upward views, nine downward views and two blackbody calibration targets to the receiver mounted inboard the aircraft. Only the view closest to zenith is used in this study. Quasi-optical elements within the receiver couple all channels onto a common view

Table 2. MARSS' Characteristics Since August 2000

Channel	89	157	183 ± 1	183 ± 3	183 ± 7
Center frequency, GHz	89.0	157	183.248	183.248	183.248
3dB limits of double passbands, GHz	0.75–1.4	1.3–3.9	0.75–1.2	2.5–3.5	6.0–8.0
Integration time, ms	100	100	100	100	100
Sensitivity NEΔT, K	0.42	0.69	0.64	0.44	0.35
Accuracy r.m.s., K (level flight)	0.88	1.09	0.98	0.86	0.81
Beam width (FWHM)	12°	11°	6.2°	6.2°	6.2°

axis. These scenes are viewed sequentially over a scan period of 3 s. The data have been checked for galactic and solar contamination by comparing adjacent upward views.

[26] Views of the calibration targets are used to derive the receiver gain and offset, which are subsequently averaged to reduce their contribution to the noise budget. The calibration was discussed in detail in [*McGrath and Hewison*, 2001]. It was concluded that the instantaneous brightness temperature accuracy ~1 K (r.m.s.) is typically achieved in level flight, when the hot calibration target is maintained 70 K above the ambient target. This is limited by the uncertainty in the brightness temperature of the hot target, due to thermal gradients through its absorber coating.

[27] Previously *McGrath and Hewison* [2001] used a radiative transfer model to provide an absolute reference for the calibration in the zenith view during high-level flight. It was believed that this could be accurately modeled from a nearby radiosonde profile, or climatology. However, the results presented here suggest the radiative transfer models can substantially underestimate T_b in cold, dry atmospheres. This has serious implications when using this method of calibration, so the method has been modified as described in the following paragraph.

[28] The "tip curve" technique [*Han and Westwater*, 2000] can be used to provide an absolute reference for a microwave radiometer measuring an optically thin atmosphere at a range of zenith angles. This was applied to all MARSS upward views during high-level flight [*Hewison and Pollard*, 2002] to derive further corrections to the hot target temperature used in the calibration. These corrections have been applied to all data used in this study. In one case, the tip curve calibration was found to produce zenith brightness temperatures of approximately 7 K in the 89, 157 and 183 ± 7 GHz channels at 7 km. These values are higher than the previous calibration based on modeled zenith radiances by 2.5 K at 89 GHz, 1.1 K at 157 GHz and 1.0 K at 183 ± 7 GHz. These corrections are broadly consistent with the bias found in the models' absorption coefficients found in typical stratospheric conditions in this study (see section 5).

[29] To exploit the available data sets, the stability of MARSS calibration during profiles was investigated. It was found that the absolute accuracy of calibrated brightness temperatures is degraded slightly (to ~1.4 K r.m.s.) because of instability in the calibration target temperature. The data sets include both ascending and descending profiles. No hysteresis was evident in the observed brightness temperatures with respect to modeled values.

[30] The 89 GHz channel initially suffered from intermittent interference problems (standing waves) due to leakage from the new 91.6 GHz oscillator being reflected back into the radiometer. This caused the 89 GHz brightness temperatures to fluctuate by ±10 K, rendering them useless for model validation. This was rectified in August 2000 by replacing the band-pass filter of this channel to one that matches that of AMSU's 89 GHz channels more closely, as shown in Table 2. Data prior to this modification have been removed from this study.

[31] Calibration target thermometry and thermal gradients and changes in the reflectivity of the scan mirror were analyzed in [*McGrath and Hewison*, 2001]. Corrections derived from this analysis have been applied to the MARSS data used here. Beam truncation by quasi-optic elements can degrade a radiometer's beam efficiency. In the case of MARSS, the 89 GHz channel is most effected because it has the broadest beam in the near field and the largest tip curve calibration corrections. It has been estimated that 95% of the power received by this channel originates within 20° of boresight. An antenna beam pattern has been synthesized as a hybrid between a Gaussian and Airy beam pattern to match this response. This was convolved with the expected map of sky T_b to estimate that this effect increases the apparent zenith T_b by ~1 K. This difference increases with angle from zenith, such that the tip curve calibration should correctly compensate for this effect to a first-order approximation. Other potential sources of observation error were analyzed and found to have negligible impact including aircraft elements contaminating the radiometer's field of view, target reflectivity and detector nonlinearity [*McGrath and Hewison*, 2001].

3.3. Aircraft Pressure Sensor

[32] Static pressure is measured on the aircraft by a Rosemount 1201F variable capacitance probe, which has a quoted accuracy of ±3 hPa. However, it is believed to

Figure 2. MARSS pod on the Met Office C-130.

perform much better than this, such that its contribution to the overall error budget of the experiment is negligible.

3.4. Aircraft Temperature Sensor

[33] Air temperature was measured on the aircraft by a Rosemount 102AL platinum resistance thermometer. A well-known correction is applied for the true air speed of the aircraft. This instrument has a quoted accuracy of ±0.5°C over the range −80°C to +40°C. As these flights were conducted in clear air, the nondeiced version of this sensor was used.

3.5. Aircraft Humidity Sensors

[34] The aircraft measured humidity in situ using a General Eastern chilled mirror dew point hygrometer and a fast response Lyman-α absorption hygrometer. The chilled mirror hygrometer relies on a thermoelectric cooler, which has a poor response time (several minutes) in dry air with a low frost point. This instrument can also suffer from ambiguity between dew point and frost point when supercooled liquid may be present on the mirror, for example, when profiling up through the freezing level. These factors make it unsuitable for acquiring ascending profiles.

[35] The Lyman-α hygrometer measures the UV radiation absorbed by water vapor. It has a much faster response time ($\ll$1 s) and provides a direct measurement of water vapor, thus overcoming the frost/dew point ambiguity. However, this instrument requires calibration against a reference. In this case, its output was compared with the General Eastern hygrometer in clear air during a descending profile to derive calibration coefficients. Its accuracy is therefore limited to that of this reference. This has been estimated as ±0.008 g/kg or ±8% (whichever is greater) for humidity mass mixing ratio, $0 < r < 20$ g/kg, based partly on previous comparison with a cryogenically cooled mirror hygrometer [*Ström et al.*, 1994]. The aircraft humidity sensors were also compared with dropsonde and radiosonde sensors [*Vance et al.*, 2004]. Humidity profiles are derived from the Lyman-α hygrometer throughout this study.

4. Comparing Observed and Modeled Brightness Temperature at Bottom of Profiles

[36] One technique commonly used to validate absorption models is to compare their predictions with observed downwelling radiances at low levels (usually at the surface). This method is applied in this section by using instantaneous data obtained at the bottom of profiles. Only profiles covering more than 500 hPa in vertical extent with a maximum pressure >950 hPa were used to represent typical surface conditions, while minimizing the influence of the atmosphere above the profile top.

[37] Instantaneous T_b measurements in profiles were found to have a lower variance from the modeled T_b than measurements taken before and after the profiles. This is due to the in situ observations being close in time and space to the radiometric measurements, otherwise the atmospheric variability dominates their random error. This technique also opens up the use of a much greater data set.

[38] The profile of pressure, temperature and specific humidity (p, T, q, respectively) from the aircraft sensors was interpolated onto a vertical grid with 2 hPa spacing. A nearby radiosonde ascent was used to "top-up" the aircraft profile to 20–30 km. The radiative transfer equation was evaluated by dividing the passbands of each channel into 22 discrete frequencies. At each frequency T_b of cosmic microwave background was defined (2) and the absorption coefficient calculated in each profile layer. The downwelling radiances at each sub frequency were then propagated down through each layer before being averaged together and converted to a channel average T_b which was compared with the observed T_b.

[39] For this study, brightness temperature, T_b, is defined to be linear with radiance, following the approach used by *English et al.* [1994], by modifying the Rayleigh-Jeans approximation to retain the second-order term of the expansion of the Planck function. This ensures the brightness temperature of a blackbody (>10 K) is equal to its thermodynamic temperature. However, this requires a frequency-dependent adjustment to the effective brightness temperature of the cosmic microwave background from its true value of $T_{CMB} = 2.73$ K to $T_{b,CMB} = 4.76$ K at 183 GHz:

$$T_{b,CMB} = \frac{h\nu}{2k}\left(\frac{e^{h\nu/kT_{CMB}}+1}{e^{h\nu/kT_{CMB}}-1}\right) \quad (2)$$

where ν is the frequency and h and k are the Planck and Boltzmann constants, respectively.

[40] Figure 3 shows the resulting differences between the seven models and the observations in five channels. The x-axes in these plots are the observed brightness temperatures, T_b, in the nominal "zenith" view (usually 12° from true zenith). Higher values represent more humid/warmer profiles. Each point represents the brightness temperature difference, ΔT_b (modeled-observed) at bottom of one profile. A few outlying points have been omitted from the plots for clarity of scales, but included in the statistics.

[41] The dotted lines in Figure 3 indicate zero bias and the 1σ uncertainty in ΔT_b introduced by errors in the humidity profile (assumed to be 8% of the IWV) and calibration errors in MARSS (1.4 K r.m.s.). The straight, solid line in each panel represents a linear regression for that model/channel combination. The r.m.s. difference and coefficients of the fit are given in the form $\Delta T_b = a + b.T_b$ in each panel.

[42] There are fewer results (13) at 89 GHz, because of interference problems experienced on earlier flights. Range of IWV = 1.2–48.2 kg/m^2. Mean = 15.6 kg/m^2. All models significantly underestimate T_b at 89 GHz to a similar extent in cold, dry arctic profiles. This suggests an important emission mechanism is not represented in the models. In warm and humid tropical profiles, the models differ more at 89 GHz. MPM93 overestimates T_b considerably because of the strong temperature dependence in its foreign broadened continuum term. This was reduced by *Rosenkranz* [1998], who reverted this component to that of MPM87. Further revision of the 118 GHz line helped make Ros03 fit observations most closely in these conditions. Without the tip curve calibration corrections, the observed T_b at 89 GHz is 5–6 K higher than these results, so the models appear less biased in cold, dry atmospheres.

[43] There are more results (33) for the higher-frequency channels, covering a wider range of IWV = 1.2–50.5 kg/m^2.

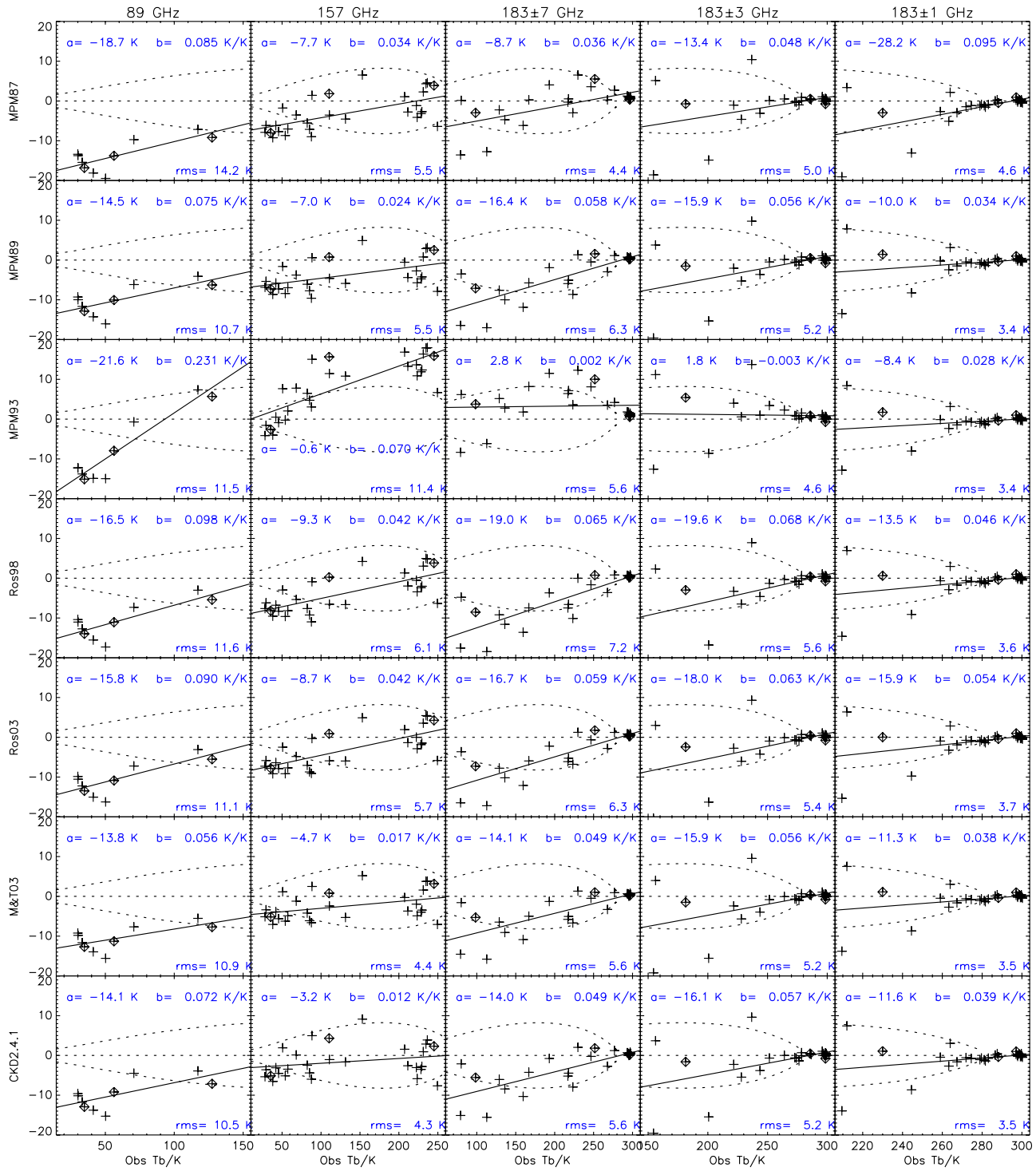

Figure 3. Modeled-observed "zenith" brightness temperature difference [K] near the surface. Columns show results for MARSS channels centered at 89, 157, 183 ± 7, 183 ± 3, and 183 ± 1 GHz. Rows show results for MPM87, MPM89, MPM93, Ros98, Ros03, M&T03, and CKD2.4.1 absorption models. Each point represents the model bias and observed zenith T_b at the bottom of one profile ($p > 950$ hPa). Dotted lines show 1σ uncertainty in T_b due to errors in the humidity profile and calibration errors in MARSS. Points enclosed in diamonds indicate "typical" arctic, midlatitude and tropical profiles used in Tables 3–5.

Mean = 20.5 kg/m^2. The tip curve calibration corrections have a much smaller impact in these channels (<1 K).

[44] The stronger continuum absorption at 157 GHz is generally better represented by the models. Although in arctic profiles, all models again significantly underestimate T_b. MPM93 fits the observations closest in cold, dry profiles, but overestimates T_b in more humid/warmer atmospheres significantly. Again, this suggests its for-

Table 3. Zenith Brightness Temperature Bias (K) Near Surface of an Arctic Profile IWV = 2.0 kg/m^2

ν, GHz	89	157	183 ± 7	183 ± 3	183 ± 1
Observed, K	34.8	35.4	98.4	181.4	230.0
MPM87	−16.8	−8.0	−3.0	−0.7	−3.0
MPM89	−12.9	−7.3	−7.1	−1.5	1.4
MPM93	−15.1	−2.6	3.8	5.4	1.7
Ros98	−14.0	−8.2	−8.5	−3.0	0.6
Ros03	−13.5	−7.8	−7.3	−2.4	0.0
M&T03	−12.7	−5.2	−5.3	−1.5	1.1
CKD2.4	−12.9	−5.1	−5.6	−1.6	1.1

Table 5. Zenith Brightness Temperature Bias (K) Near Surface of a Tropical Profile IWV = 48.2 kg/m^2

ν, GHz	89	157	183 ± 7	183 ± 3	183 ± 1
Observed, K	127.4	245.0	296.4	298.5	297.1
MPM87	−9.2	3.9	0.4	−0.8	0.9
MPM89	−6.3	2.5	0.2	−0.8	1.0
MPM93	5.7	15.9	0.6	−0.7	1.0
Ros98	−5.4	3.8	0.2	−0.8	1.0
Ros03	−5.5	4.3	0.3	−0.8	1.0
M&T03	−7.7	3.2	0.2	−0.8	1.0
CKD2.4	−7.1	2.3	0.2	−0.8	1.0

eign-broadened water vapor continuum is too strong at high temperatures. Other models do well at 157 GHz in these conditions, and the CKD2.4.1 continuum provides the best fit overall.

[45] The models converge to the observations for all 183 GHz channels at high T_b, which correspond to humid, optically thick atmospheres where T_b is not sensitive to the absorption model. Some of the fitted lines for the 183 ± 1 and 183 ± 3 GHz channels are dominated outliers. However, no cause could be identified for these to have a larger bias than others, so they have been included in the results. If they are excluded, the slope of these channels' bias is not significantly different from zero. In drier atmospheres, MPM89, Ros98, Ros03 and CKD2.4.1 underestimate the absorption coefficient at 183 ± 7 GHz, which has a significant contribution from the water vapor continuum. MPM93 provides the closest overall fit to 183 GHz channels' observations in terms of bias, but may slightly overestimate T_b at 183 ± 7 GHz because of its strong continuum. Of the remaining models, the original 183 GHz line parameters used in MPM87 seem to give the best fit to the observations away from the line centre. It also appears that the modifications to the pressure broadening and line shift in Ros03 produce an improvement over Ros98.

[46] Tables 3–5 show the T_b observed at the bottom of typical arctic, midlatitude and tropical profiles, respectively, and the differences of each model's prediction from these. These profiles were selected to fall close to the best fit lines in Figure 3 in different environmental conditions. These results are not consistent with those reported by *Racette et al.* [2005], who found Ros98 to have a small positive bias (<2 K) at 90 GHz and negligible biases at 150 and 183 ± 7 GHz in arctic winter conditions. However, they also found MPM93 overestimated T_b at 150 GHz and 183 ± 7 GHz, while all models showed large positive biases at 183 ± 3 and ±1 GHz, which was attributed to a bias due to their radiosondes' being launched in an urban area of higher temperatures and humidity than the radiometer's site.

Table 4. Zenith Brightness Temperature Bias (K) Near Surface of a Midlatitude Profile IWV = 12.2 kg/m^2

ν, GHz	89	157	183 ± 7	183 ± 3	183 ± 1
Observed, K	56.3	110.4	251.6	285.8	288.1
MPM87	−13.8	1.8	5.5	0.5	−0.5
MPM89	−10.0	0.7	1.6	0.5	−0.4
MPM93	−8.0	15.6	10.0	0.9	−0.4
Ros98	−11.0	0.3	0.8	0.4	−0.4
Ros03	−10.9	0.9	1.8	0.5	−0.4
M&T03	−11.3	0.8	1.0	0.4	−0.4
CKD2.4	−9.2	4.3	1.8	0.4	−0.4

5. Comparing Absorption in Profiles

[47] Although the method of analysis described in the previous section provides a useful test of the models' performance, it provides little insight into the specific shortcomings of each model, and is dominated by emission in the lower troposphere.

[48] To investigate further, MARSS' observations during profile ascents/descents can be used. It was found that, although the absolute accuracy of MARSS' calibrated brightness temperatures in profiles is degraded slightly because of instability in the calibration target temperature, this systematic bias changes only slowly with time or temperature. Therefore the relative accuracy of the brightness temperatures measured at closely spaced intervals during a profile is dominated by random noise introduced by the radiometer itself (0.5–0.8 K). This allows the absorption coefficient to be calculated from two such measurements as:

$$\alpha(p_j) = \ln\left(\frac{T_b(p_j - \Delta p) - \overline{T(p_j \pm \Delta p)}}{T_b(p_j + \Delta p) - \overline{T(p_j \pm \Delta p)}}\right) \cdot \frac{1}{2\Delta p.\sec\theta} \quad (3)$$

where

$\alpha(p_j)$ = absorption coefficient calculated at pressure, p_j,

$T_b(p)$ = T_b measured at pressure, p,

$\overline{T(p_j \pm \Delta p)}$ = average air temperature over layer,

$2\Delta p.\sec\theta$ = slant path through layer thickness, $2\Delta p$.

Δp was adjusted for each combination of channel and humidity in the range $5 \leq \Delta p \leq 200$ hPa to produce an absorption, $\alpha \sim 1$ dB, to ensure layers are not optically thick, but are thick enough to produce measurable extinction.

[49] Profiles of modeled T_b were calculated by the process described in section 4. Absorption coefficients were then calculated over $2\Delta p$ layers from the modeled and observed T_b profiles using (3). The model bias was calculated as a percentage of the observed absorption and its uncertainty was estimated assuming 0.5 K relative uncertainty on $T_b(p_j \pm \Delta p)$, and 8% uncertainty on the specific humidity, q. Although this is referred to as model bias, it includes any residual bias in the observations.

[50] This method accounts for the finite bandwidth of the instruments, which would not be accounted for if α was

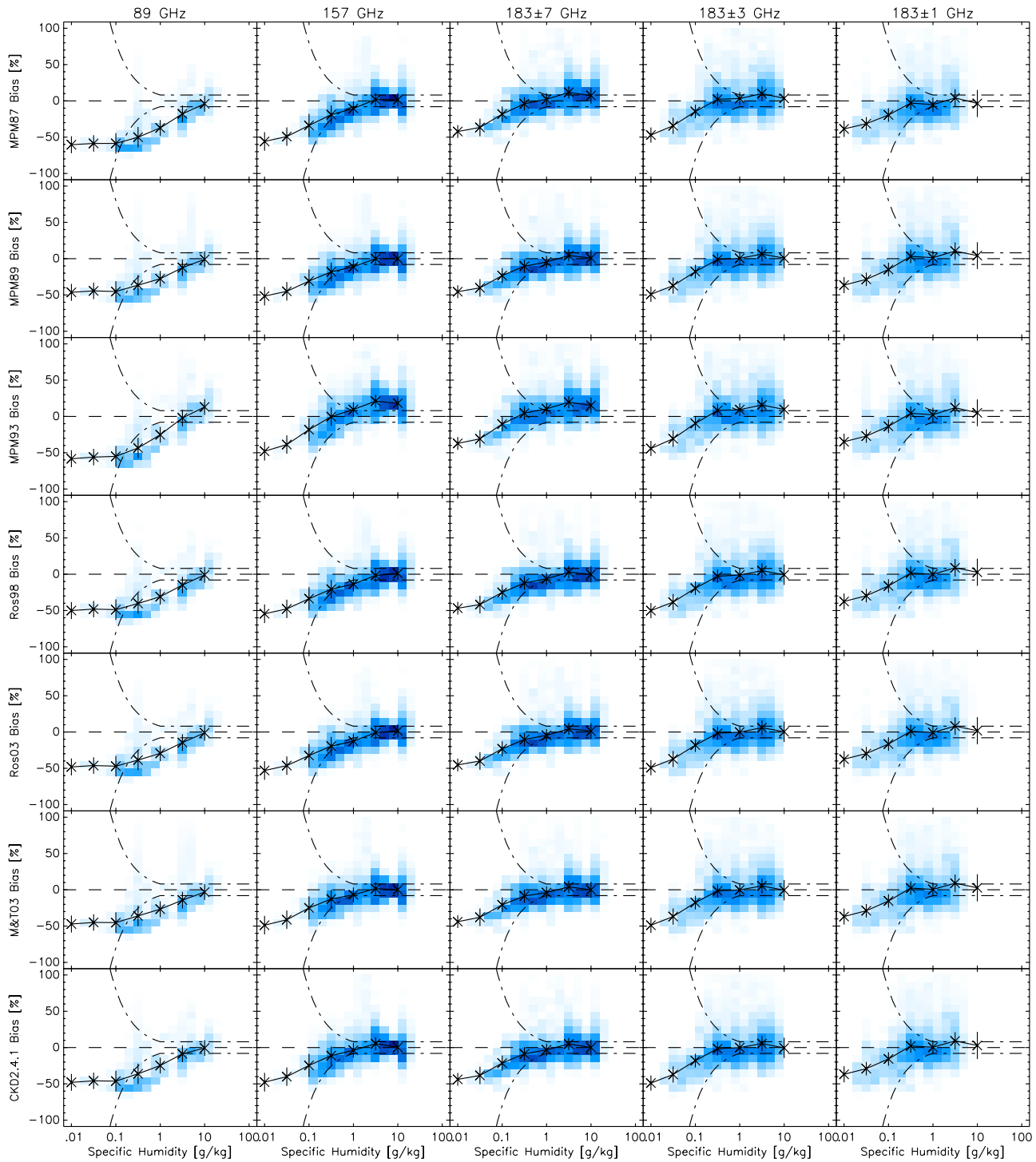

Figure 4. Percentage bias in modeled absorption coefficient with respect to observations as a function of humidity. Shading indicates data density. Darker areas correspond to most observations. Points with error bars show weighted average and SD of all observations in seven logarithmic humidity bins. Columns show results for MARSS channels centered at 89, 157, 183 ± 7, 183 ± 3, and 183 ± 1 GHz. Rows show results for MPM87, MPM89, MPM93, Ros98, Ros03, M&T03, and CKD2.4.1 absorption models. Dot-dashed lines show 1σ uncertainty in bias due to errors in the humidity profile and radiometric noise.

simply calculated from the model at a representative frequency. It is important to account for this near 183 GHz, where absorption changes nonlinearly with frequency across the passbands.

[51] Figure 4 shows the bias in α calculated from each of the seven models as a fraction of α calculated from measurements in each of MARSS' five channels. Each panel shows the percentage bias plotted against the mean

Table 6. Average Observed Absorption Coefficient and Model Absorption Bias (%) and Standard Error (%) wrt Observations at Specific Humidity, q = 0.1 g/kg

ν, GHz	89	157	183 ± 7	183 ± 3	183 ± 1
Observed, dB/km	0.15	0.13	0.36	0.90	2.33
Δp, hPa	100	100	50	20	20
MPM87	−58.7	−33.9	−18.1	−14.6	−19.5
MPM89	−45.3	−30.9	−23.3	−17.9	−14.9
MPM93	−55.0	−18.2	−10.5	−9.6	−13.7
Ros98	−48.8	−33.8	−25.0	−19.2	−16.2
Ros03	−47.0	−32.4	−23.2	−18.1	−16.6
M&T03	−45.1	−25.0	−20.7	−17.6	−15.4
CKD2.4	−46.3	−24.5	−21.4	−18.0	−15.7
Standard error	0.8	0.7	0.4	0.3	0.3

Table 8. Average Observed Absorption Coefficient and Model Absorption Bias (%) and Standard Error (%) wrt Observations at Specific Humidity, q = 10 g/kg

ν, GHz	89	157	183 ± 7	183 ± 3	183 ± 1
Observed, dB/km	0.99	4.21	16.9	25.9	44.4
Δp, hPa	10	10	10	5	5
MPM87	−4.0	+1.5	+7.3	+3.5	−3.6
MPM89	−0.9	−0.2	+0.7	+0.7	+4.2
MPM93	+13.1	+18.2	+15.2	+9.6	+5.1
Ros98	−1.0	+1.0	−0.2	−0.7	+2.7
Ros03	−1.1	+1.6	+1.3	+0.3	+1.8
M&T03	−3.2	+0.1	−0.1	−0.5	+2.7
CKD2.4	−0.6	+0.4	+0.1	−0.4	+2.9
Standard error	0.5	0.2	0.3	0.6	3.8

specific humidity, q, for all layers of the profiles. Only results with calculated uncertainty <0.5α are included. This results in different data densities for each channel as the 183 GHz channels become optically thick at high q, even for Δp = 5 hPa, and window channels are dominated by radiometric noise at low q, even for Δp = 200 hPa, which limits the range of average q. There are too many points to show individually (∼5000), so the results are plotted as 2D histograms, where the shading represents the density of observations, white being none, the darkest shades represent more than 160 observations in each bin (10% bias) × (5 dB humidity). Again, there are fewer results at 89 GHz (∼2000). The relationships between model bias and temperature and pressure have also been examined, but were found to be less well correlated.

[52] The crosses and vertical error bars in Figure 4 represent the average and standard deviation of the bias, weighted statistically by the variance estimate, in seven bins, each 5 dB wide in $\log_{10}(q)$. The average bias in each bin is not necessarily equal to the modal value, and is connected for illustration only; this shows the bias changes continuously with humidity. The mean biases and their statistical uncertainty at 3 values of q are also tabulated in Tables 6–8 together with the average observed α in these conditions.

[53] The first two columns of Figure 4 show all models seriously underestimate the observed α at 89 GHz and 157 GHz at low humidity. This is consistent with the negative bias in T_b found in these channels. Although this negative bias is within the nominal uncertainty of the humidity (±0.08 g/kg) at low q, it persists even when the profiles are saturated artificially. In more humid conditions, the models predict the measured absorption more accurately. This trend is also evident in the 183 GHz channels, although with less magnitude.

Table 7. Average Observed Absorption Coefficient and Model Absorption Bias (%) and Standard Error (%) wrt Observations at Specific Humidity, q = 1 g/kg

ν, GHz	89	157	183 ± 7	183 ± 3	183 ± 1
Observed, dB/km	0.25	0.43	2.02	5.57	12.7
Δp, hPa	100	50	50	20	20
MPM87	−37.2	−10.5	+2.2	+3.2	−5.2
MPM89	−27.7	−11.3	−4.6	+0.4	+1.4
MPM93	−25.3	+9.5	+10.5	+9.3	+2.3
Ros98	−31.0	−13.6	−6.2	−1.1	0.0
Ros03	−29.4	−12.6	−4.6	−0.1	−0.7
M&T03	−26.7	−6.9	−3.8	−0.2	+0.5
CKD2.4	−24.8	−3.8	−3.1	−0.0	+0.5
Standard error	0.6	0.3	0.2	0.2	0.2

[54] At 89 GHz, in dry conditions, the modeled absorption is dominated by oxygen, and is quite similar in the different models. They have a negative average bias of ∼50% in low specific humidity ($q \leq 0.1$ g/kg). It is also significantly larger than the uncertainty in q for medium humidity ($q \sim 1$ g/kg). This bias decreases at higher humidity; at $q \sim 10$ g/kg MPM89, Ros98, Ros03 and CKD2.4.1 are found to be unbiased within the uncertainty. However, MPM93 overestimates α by 12% in these conditions, because of the strong foreign broadened water vapor continuum, as a result of its high temperature coefficient. This model shows similar positive bias in the 157 and 183 ± 7 GHz channels, where the water vapor continuum is also significant.

[55] At 157 GHz, the absorption is dominated by the water vapor continuum; the self-broadened part typically becomes dominant for $q > 10$ g/kg. In very dry conditions, the N_2 continuum is also significant. Again, all models show a strong deficit (∼50%) for $q < 0.1$ g/kg and are quite similar. For $q \sim 1$ g/kg, the CKD2.4.1 continuum is less biased (−23%) than MPM89, Ros98 or Ros03, which are very similar (∼12%). In more humid conditions, ($q \sim 10$ g/kg), the models all show a small bias (<2%), although MPM93 again overestimates (by 18%).

[56] All models again underestimate α measured in all the 183 GHz channels in dry conditions, but this bias reduces in higher humidity and is of lower magnitude near the line center, as the opacity increases. In the most humid conditions ($q \sim 10$ g/kg), MPM87 has a small positive bias (∼4%) at 183 ± 7 and ±3 GHz. These biases were corrected by the adjustments to the 183 GHz line made in MPM89, which is almost unbiased here. However, it is slightly more biased than its predecessor in low humidity away from the line centre. Ros98 produces very similar results to MPM89 at all frequencies tested. However, the modifications introduced in Ros03 have brought some small reductions in bias, most noticeable at 183 GHz for $q \sim 0.03$ g/kg. Over the full humidity range, MPM93 produces the lowest average absorption bias, except at 89 GHz. However, this should not be taken as an endorsement of this model, as it was

found to produce more biased T_bs, because of the dominance of emission from the lower troposphere.

[57] When the tip curve calibration corrections are not applied to the observed T_bs, the absorption bias results are very similar, except for moderate humidity ($q \sim 1$ g/kg) at 89 GHz, where the bias is reduced by ~12%, though still significant compared to the expected uncertainty for all models. The tip curve corrections have less impact at 89 GHz at lower and higher humidity and at higher frequencies (~1% at 157 GHz).

6. Conclusions

[58] This paper compares observations made with a Microwave Airborne Radiometer Scanning System (MARSS) with various absorption models. The data set includes 33 profiles covering a range of conditions from tropical to arctic. A subset of this data set has been used to validate infrared absorption models using measurements from an interferometer on the same aircraft [*Taylor et al.*, 2003]. Low-level zenith infrared observations in the tropics suggest the self-broadening coefficient of the CKD2.4 water vapor continuum is too strong by 6–15%, dependent on frequency. The same model had negligible bias in arctic conditions (due to negligible absorption). These results are not inconsistent with my findings in the microwave, as a nonlinear frequency-dependent bias was found in the infrared, which cannot be extrapolated to microwave frequencies. Also, the IR results were based only on low-level observations, which are dominated by emission in the warmer, lower troposphere. In these conditions, negligible bias was found when applying the CKD model to millimeter wavelengths.

[59] Ground-based microwave radiometers may operate at the frequencies used in this study for cloud observations and humidity profiling, especially in the arctic, where the more commonly used 22 GHz line does not provide sufficient sensitivity. In such cold conditions, all models and retrievals based on them may be biased. In tropical conditions, however, MPM93 will overestimate absorption and hence the brightness temperature in window channels. These channels are also commonly used for humidity sounding from space. The 183 GHz channels are usually well modeled and emission in the window channels at 89 and 157 GHz is dominated by the atmosphere near the surface and is also accurately modeled in warm, humid conditions, except by MPM93. In cold, arctic conditions all models underestimate absorption in the window channels. However, this may not be obvious as the use of these data is currently limited because of the variability of the surface emissivity in the same regions.

[60] These results are not consistent with the suggestion from *Wessel and Boucher* [1998] that the strength of the water vapor continuum needs to be increased by 9% in MPM89, on the basis of comparison of SSM/I and SSM/T-2 data over the tropical south Pacific, as I found this model to be unbiased in these conditions. However, *Rosenkranz and Barnet* [2006] found no significant bias in the Ros03 model when comparing accurate, collocated radiosondes with 150 GHz and 183 GHz observations from the Humidity Sounder for Brazil (HSB) in tropical and midlatitude sites. The results presented in this paper are also in contrast to observations from an earlier version of MARSS [*English et al.*, 1994]. This is partly due to the revised calibration procedure introduced since the discovery of the MPM89's bias in cold, dry conditions, which had previously been used as a calibration reference point. It is also believed that use of radiometric data in profiles has not only extended the available data set, but also reduced errors of representation, which otherwise dominate the error budget of such a comparison.

[61] The observed absorption bias at low specific humidity suggests the mechanism responsible for absorption is not adequately represented in the current generation of models. There has been some discussion about the accuracy of the oxygen line coupling coefficients when extrapolated to temperatures below 0°C [*Boukabara et al.*, 2005; *Rosenkranz*, 2005]. This may explain some of the bias found at 89 GHz, where it is most serious, but less at 157 GHz, and none at 183 GHz. This bias may also be due to the influence of an emission line not represented in the models, an erroneous temperature coefficient in the foreign broadened term of the water vapor continuum or a continuum term from another species. These possibilities should be considered in more detail, for example in the analysis of data from laboratory data, which have now been obtained at low temperatures [*Meshkov and De Lucia*, 2005]. However, given the large corrections to the 89 GHz channel found necessary in this study, there remains a possibility that the results of this channel could be explained by observational errors. Other investigators are urged to also consider calibration completely independent of absorption models to verify these results.

[62] **Acknowledgments.** I am indebted to the dedication and skill of the staff that operated and supported the Met Office C-130, including the ground and aircrew. I would also like to thank the reviewers of this paper, Christian Mätzler and Peter Rayer, for their comments, as well as Phil Rosenkranz, who also supplied the code for his new absorption model.

References

Boukabara, S.-A., S. A. Clough, J.-L. Moncet, A. F. Krupnov, M. Tretyakov, and V. V. Parshin (2005), Uncertainties in the temperature dependence of the line coupling parameters of the microwave oxygen band: Impact study, *IEEE Trans. Geosci. Remote Sens.*, *43*(5), 1109–1114.

Cimini, D., E. R. Westwater, Y. Han, and S. Keihm (2003), Accuracy of ground-based microwave radiometer and balloon-borne measurements during the WVIOP2000 field experiment, *IEEE Trans. Geosci. Remote Sens.*, *31*(11), 2605–2615.

Clough, S. A., F. X. Kneizys, and R. W. Davies (1989), Line shape and the water vapor continuum, *Atmos. Res.*, *23*, 229–241.

Edwards, D. P. (1992), GENLN2: A general line-by-line atmospheric transmittance and radiance model, *NCAR Tech. Note TN376*, Natl. Cent. for Atmos. Res., Boulder, Colo.

English, S. J., C. Guillou, C. Prigent, and D. C. Jones (1994), Aircraft measurements of water vapor continuum absorption, *Q. J. R. Meteorol. Soc.*, *120*, 603–625.

English, S. J., D. C. Jones, P. J. Rayer, T. J. Hewison, R. W. Saunders, C. Guillou, C. Prigent, J. Wang, and G. Anderson (1995), Observations of water vapor absorption using airborne microwave radiometers at 89 and 157 GHz, *Proc. IGARSS'95 Geosci. Remote Sens. Symp.*, *2*, 1395–1397.

Han, Y., and E. R. Westwater (2000), Analysis and improvement of tipping calibration for ground-based microwave radiometers, *IEEE Trans. Geosci. Remote Sens.*, *38*(3), 1260–1276.

Hewison, T. J., and D. F. Pollard (2002), Calibrating MARSS by the tip curve method, *MRF Tech. Note 42*, Met Office, Exeter, U. K.

Krupnov, A. F., G. Y. Golubiatnikov, V. N. Markov, and D. A. Sergeev (2002), Pressure broadening of the rotational line of oxygen at 425 GHz, *J. Mol. Spectrosc.*, *215*(2), 309–311.

Liebe, H. J. (1989), MPM—An atmospheric millimeter wave propagation model, *Int. J. Infrared Millimeter Waves*, *10*(6), 631–650.

Liebe, H. J., and D. H. Layton (1987), Millimeter-wave properties of the atmosphere: Laboratory studies and propagation modeling, *NTIA Rep. 87-224*, Natl. Telecommun. and Inf. Admin., Boulder, Colo.

Liebe, H. J., P. W. Rosenkranz, and G. A. Hufford (1992), Atmospheric 60-GHz oxygen spectrum: New laboratory measurements and line parameters, *J. Quant. Spectrosc. Radiat. Transfer*, *45*(5/6), 629–643.

Liebe, H. J., G. A. Hufford, and M. G. Cotton (1993), Propagation modeling of moist air and suspended water/ice particles at frequencies below 1000 GHz, paper presented at 52nd Specialists' Meeting of the Electromagnetic Wave Propagation Panel, Advis. Group for Aerosp. Res. and Dev., Palma de Mallorca, Spain.

Ma, Q., and R. H. Tipping (2003), A simple analytical parameterization for the water vapor millimeter wave foreign continuum, *J. Quant. Spectrosc. Radiat. Transfer*, *82*, 517–531.

McGrath, A. J., and T. J. Hewison (2001), Measuring the accuracy of a Microwave Airborne Radiometer (MARSS), *J. Atmos. Oceanic Technol.*, *18*(12), 2003–2012.

Meshkov, A. I., and F. C. De Lucia (2005), Broadband absolute absorption measurements of atmospheric continua with millimeter wave cavity ringdown spectroscopy, *Rev. Sci. Instrum.*, *76*(8), 083103.

Pardo, J. R., E. Serabyn, and J. Cernicharo (2001), Submillimeter atmospheric transmission measurements on Mauna Kea during extremely dry El Nino conditions: Implications for broadband opacity contributions, *J. Quant. Spectrosc. Radiat. Transfer*, *68*, 419–433.

Racette, P. E., et al. (2005), Measurement of low amounts of precipitable water vapor using ground-based millimeterwave radiometry, *J. Atmos. Oceanic Technol.*, *22*, 317–337.

Rayer, P. J. (2001), Microwave transmittance models for RTTOV, report, Met Office, Exeter, U. K. (Available at http://www.metoffice.com/research/interproj/nwpsaf/rtm/index.html)

Rosenkranz, P. W. (1993), Absorption of microwaves by atmospheric gases, in *Atmospheric Remote Sensing by Microwave Radiometry*, edited by M. A. Janssen, pp. 37–90, John Wiley, Hoboken, N. J.

Rosenkranz, P. W. (1998), Water vapor microwave continuum absorption: A comparison of measurements and models, *Radio Sci.*, *33*(4), 919–928, (Correction, *Radio Sci.*, *34*(4), 1025, 1999.)

Rosenkranz, P. W. (2005), Comment on "Uncertainties in the temperature dependence of the line-coupling parameters of the microwave oxygen band: Impact study", *IEEE Trans Geosci. Remote Sens.*, *43*(9), 2160–2161.

Rosenkranz, P. W., and C. D. Barnet (2006), Microwave radiative transfer model validation, *J. Geophys. Res.*, *111*, D09S07, doi:10.1029/2005JD006008.

Rothman, L. S., et al. (1992), The Hitran molecular database: Editions of 1991 and 1992, *J. Quant. Spectrosc. Radiat. Transfer*, *48*, 469–507.

Ström, J., R. Busen, M. Quante, B. Guillemet, P. R. A. Brown, and J. Heintzenberg (1994), Pre-EUCREX intercomparison of airborne humidity measuring instruments, *J. Atmos. Oceanic Technol.*, *11*(5), 1392–1399.

Taylor, J. P., S. M. Newman, T. J. Hewison, and A. J. McGrath (2003), Water vapor line and continuum absorption in the thermal infrared—Reconciling models and observations, *Q. J. R. Meteorol. Soc.*, *129*(594), 2949–2969.

Tretyakov, M. Y., G. Y. Golubiatnikov, V. V. Parshin, M. A. Koshelev, S. E. Myasnikova, A. F. Krupnov, and P. W. Rosenkranz (2004), Experimental study of the line mixing coefficient for 118.75 GHz oxygen line, *J. Mol. Spectrosc.*, *223*(1), 31–38.

Vance, A. K., J. P. Taylor, T. J. Hewison, and J. Elms (2004), Comparison of in-situ humidity data from aircraft, dropsonde and radiosonde, *J. Atmos. Oceanic Technol.*, *21*, 921–932.

Wessel, J. E., and D. Boucher (1998), Comparison between cross-track and conical scanning microwave window channels near 89 GHz, *IEEE Trans. Geosci. Remote Sens.*, *36*(1), 16–24.

Westwater, E. R., Y. Han, M. D. Shupe, and S. Y. Matrosov (2001), Analysis of integrated cloud liquid and precipitable water vapor retrievals from microwave radiometers during the Surface Heat Budget of the Arctic Ocean project, *J. Geophys. Res.*, *106*(D23), 32,019–32,030.

Westwater, E. R., B. Stankov, D. Cimini, Y. Han, J. A. Shaw, B. M. Lesht, and C. N. Long (2003), Radiosonde humidity soundings and microwave radiometers during Nauru99, *J. Atmos. Oceanic Technol.*, *20*(7), 953–971.

T. J. Hewison, Met Office, University of Reading, Meteorology Building 1U20, Earley Gate, Reading RG6 6BB, UK. (tim.hewison@metoffice.gov.uk)